Solvation dynamics in liquids and glasses

Lazonder, Kees; Wiersma, D. A.

Chapter 6

Liquid/Glass Solvent Dynamics: from 300 to 3 K

In this chapter the temperature dependence of the optical non-linear response of a dye dissolved in a glass-forming liquid is studied within the context of the multi-mode Brownian oscillator model. As the frequency – frequency time correlation function of a chromophore dissolved in a glass exhibits a femtosecond component at higher temperatures, femtosecond pulses are to be used in these experiments. The results of temperature-dependent echo-peakshift and heterodyned echo experiments in glass-forming liquids are discussed. Freezing out a large part of the bath fluctuations by varying the temperature from 300 K to 3 K allows for testing current solvation models.

6.1 Introduction

In the previous chapter solvation dynamics of glasses have been studied in the temperature realm of the two-level system (TLS) theory, were chromophores are supposed to couple to nearly degenerate double wells in the potential energy landscape. By charting the time-resolved correlation function of optical transitions upon ultrashort excitation, detailed insight into the dynamics of the solvent was obtained. However, at higher temperatures the TLS description of these dynamics becomes inadequate. Coupling of the chromophore to local phonon modes and other collective relaxation mechanisms becomes dominant as the temperature increases [94,117,134,180,242,261]. At room temperature, above the glass

transition for the solvents studied in this work, the description of the solvation dynamics usually follows the lines of the multi-mode Brownian oscillator (MBO) theory, as introduced in section 2.3. It models the chromophore – solvent interactions by assuming an electronic transition that is linearly coupled to a bath of harmonic oscillators.

The MBO model [55,146,147,152,153] which was successfully used to describe the solvent dynamics at room temperatures in the liquid phase, has also been tested at lower temperatures. All studies on temperature dependent solvation dynamics have been conducted in polymer hosts that form an amorphous solid already at room temperature. With respect to the bath dynamics, the polymer host can be considered as similar to a glass. However, no glass transition occurs in the temperature ranges that were studied, and experimentally, no major deviations from theoretical predictions for the linebroadening were reported.

Weiner *et al.* were the first to study the temperature dependence of the three pulse echo peakshift (3PEPS) in a glass host [168,169]. In the 3PEPS experiment, the offset of the waiting time between the second and the third pulse and/or the maximum of the time-integrated echo signal from zero delay is measured as a function of the temperature. A linear increase of ~30 fs of the echo peakshift was found with decreasing temperature when cooling a polymethyl methacrylate (PMMA) sample doped with cresyl violet from 290 K to 15 K. This was explained as a transition from homogeneous to inhomogeneous broadening due to smearing of the vibrational structure of individual dye molecules. Despite the clearly resolved peakshift in the low temperature scattering data, a pronounced echo tail, indicative of a long dephasing time T_2, was not observed. The waiting time measurements did not show any appreciable changes in the echo peak position which was interpreted as indication that spectral diffusion does not play a major role in the polymer matrix.

In a later study by Bardeen *et al.* [151,262] the two-pulse echo (2PE) and the three-pulse echo (3PE) response of two other dyes, Oxazine 4 and Styryl 7, dissolved in both PMMA and polyvinyl alcohol (PVA) were measured for temperatures from 30 K to 300 K. The echo decays in the case of the Styryl dye were too fast to be discussed in a meaningful way at any temperature. In the case of the Oxazine dye, the signal was interpreted as a combination of one dominant vibrational mode and a single exponential decay of the polarization. A linear dependence of the dephasing rate associated with this exponential decay with temperature was found. The authors note that this is consistent with linear coupling of the transition to the phonon bath when the high-temperature limit (i.e. $kT >> \hbar\omega$) is valid for all phonons at all temperatures. This implies that the dephasing is caused by low frequency modes, that is, by those modes whose frequencies lie below $20\ \mathrm{cm}^{-1}$. However, the dephasing time caused by these modes found in the echo decays is ~ 50 fs, which corresponds to phonon frequencies in the range of $1000\ \mathrm{cm}^{-1}$. Therefore, the system's frequency fluctuations appear to be Markovian when the correlation time is considered, and should thus be

described using high frequency modes. Hence, there exists an apparent incongruity between the linear temperature dependence of the dephasing rates and the Markovian character of the echo decays. The authors suggested that the linear coupling representation as implied by the MBO model is inadequate, and that quadratic or higher coupling terms need to be considered.

On the other hand, Nagasawa *et al.* [149,150,263] concluded that the MBO model should still be readily applicable to describe the optical dephasing of the infrared dyes IR144 and DTTCI dissolved in polyvinylformal (PVF) and PMMA down to temperatures of 30 K. Besides considering the 3PE signal and the absorption spectrum, they also studied the 3PEPS and transient grating scattering, which afforded a more detailed analysis of the temperature dependence of the modes involved in the optical dephasing process. The experiments revealed an initial decay of the peakshift that could be modeled by assuming fast dephasing of intramolecular vibrational wave packets and an inertial solvent response, followed by quantum beats originating from the prominent intramolecular modes of the dye. Nagasawa *et al.* found that in these glasses the inertial response was best modeled using a severely damped oscillator to allow for some undershoot in the peakshift data. At the same time they indicate that the precise characterization of this mode is limited by the resolution obtained in the analysis of the experimental data. Contrary to the experiments by Bardeen *et al.*, the detailed computer simulations showed that the peakshift signal and also the absorption and Raman spectra could be self-consistently reproduced at all temperatures, by assuming a fixed spectral density in terms of the MBO model.

Furthermore, according to the experiments by Nagasawa *et al.* the relatively weak coupling of DTTCI to its vibrational and bath modes results in a more prominent temperature dependence of the peakshift when compared with other dyes like IR 144. On the other hand the temperature dependence of the residual peakshift at long waiting times of the sample containing IR144 dissolved in PVF showed an unexpected maximum at temperatures around 100 K that, according to the authors, could not be accounted for within the framework of the harmonic bath model. However, later calculations by the same authors demonstrated that this feature originates solely from the effects of finite pulse widths, namely the temperature-dependent detuning between the laser and transition frequencies which was not initially taken into the consideration [150]. If these effects are included properly in the calculations, no major deviations from the MBO model are observed.

Optical dephasing of zinc-octaethylporphine in several glass forming liquids at temperature from 0.35 K to a maximum of 100 K was investigated by Vainer and Gruzdev *et al.* [134,261,264-267] using narrowband two-pulse and incoherent photon echoes. They were able to distinguish between a low temperature range, where dephasing mechanisms related to tunneling TLSs were dominant, and a higher temperature range where the dephasing was

best described by the coupling of the chromophore to one or two low frequency vibrational bath modes.

Almost all previously reported studies concentrated on polymer solvents that show no phase transition in the temperature range under consideration. Only the above mentioned narrowband studies by Vainer and Gruzdev *et al.* used a simple glass forming liquid and a wide temperature range, but also these studies were conducted at temperatures that were below the glass transition at all instances. The effect of a phase transition was not investigated.

In this chapter the temperature dependence of solvent dynamics in a glass forming host is studied using a number of femtosecond four-wave mixing (such as 3PE, 3PEPS and heterodyne detected photon echoes, HDPE) and steady-state spectroscopic techniques from room temperature down to the cryogenic regime. This temperature range includes a phase transition at 150 K where all diffusive solvent motion slows down to a completely static state of affairs. It is shown that the HDPE technique is far more sensitive to the changes of these parameters than the 3PEPS experiment is. In particular, the glass transition is hardly noticeable in the temperature dependent 3PEPS experiment at moderately long times, when it can be clearly seen in the temperature dependent HDPE data.

The ability of the MBO-model to accommodate temperature changes with a temperature independent spectral density (SD) is tested. It is found that it is not possible to account for the experimental results with a fixed SD even over relatively moderate temperature ranges. The parameters of the Brownian oscillator modes (BO's) that are used for describing the third-order optical response of the system at room temperature clearly exhibit temperature dependence, thus changing the SD of the system. The lack of diffusive motion below the glass transition does not exclude all dynamics at these temperatures, as the remaining intramolecular modes and some residual inertial solvent modes still cause coherence loss at short times. The temperature dependence of the MBO parameters matches largely the expected temperature dependence of the microscopical physical processes that underlie the modes in question. However the fastest mode that is frequently associated with dephasing of the vibronic manifolds does not depend on temperature in a way that is characteristic for the vibronic dephasing. Instead, this mode is attributed to quadratic or anharmonic coupling of pseudo-local phonon modes to the electronic transition, since its temperature dependence ties in with such or a similar mechanisms much better.

6.2 Experimental Results

An overview of the main experiments that are considered when obtaining the correlation function and SD is displayed in Figure 6.1. These plots are meant to give a concise outline of the effects of temperature on the outcome of the various experiments. The glass forming liquid of choice is a 1:1 volume mixture of ethanol and 1,2 propanediol (EtOH/PD) because this mixture yields glass samples of good optical quality upon rapid cooling. The infrared dye DTTCI was picked for its absorption spectrum that has an excellent overlap with the spectrum of the excitation pulses. It also has a low number of low-frequency vibrational modes relative to other laser dyes in the same frequency range.

The absorption spectrum of DTTCI in EtOH/PD in Figure 6.1.a shows the narrowing of the width of the spectrum with decreasing temperature. Where at 300 K the full width at half maximum (FWHM) of the spectrum is approximately $450\ cm^{-1}$, at 100 K this is reduced to $\cong 330\ cm^{-1}$ and at 3 K it is only $\cong 260\ cm^{-1}$. The spectrum also exhibits a small red-shift of $\cong 65\ cm^{-1}$ at the lower temperatures.

Typical time-integrated three pulse echo signals at various temperatures, from which the peakshift can be deduced, are shown in Figure 6.1.b. The increasing inhomogeneous character of the solvation dynamics with decreasing temperature is obvious from the echo signal. The signal becomes wider and more asymmetric and it peaks at a later time. Whereas at 300 K the echo is approximately 40 fs wide, at 3 K this has become $\cong 80$ fs at FWHM. The echo maximum shifts from nearly 9 fs at room temperature to over 22 fs at 3 K. Although the echo stretches to longer times at lower temperatures, the nanosecond decays observed in the experiments with picosecond pulses are not present here.

The peakshift measurements as a function of the waiting time reflect the above temperature dependence as illustrated by Figure 6.1.c. As the temperature drops, the dynamics become visibly slower, and correspondingly the peakshift increases. The signal is characterized by a fast inertial-like decay at short times that at first glance seems to be temperature independent. A region that is characterized by several recurrences of the peakshift follows this decay. These quantum beats, which are caused by the intramolecular vibrational motions of the chromophore, do not change their frequency substantially at lower temperature but seem to increase in amplitude while the damping of the vibrations seems to slow down. The long tail of the peakshift signal is an indication of the coupling of the chromophore to diffusional modes of the solvent. This part of the peakshift function shows the increased "inhomogeneous" portion of the correlation function with decreasing temperature by becoming nearly constant. This decreased slope of the 3PEPS function at times longer than 2 ps clearly indicates that the modes related to diffusional solvent motion are frozen out.

The effects of temperature on the vibrational dynamics are best observed in the longitudinal dimension of the homodyne echo traces as displayed in Figure 6.1.d. The quantum beats become more prominent at lower temperatures although little seems to change as soon as the glass temperature is passed ($T_g = 150$ K). Note that this lack of change below T_g is the first signature of the glass transition that is apparent from superficial inspection of the experimental data (*vide infra*). Fitting the traces with exponentially-damped cosine functions yields the relative amplitudes, frequencies and decays of the three main vibrational modes: 0.9, 150 cm^{-1}, 150 fs; 0.03, 380 cm^{-1}, 500 fs; and 0.07, 485 cm^{-1}, 700 fs, respectively. These values corroborate well with the previously published data [177,268-270], and will be rectified later while applying the full-scale modeling. As has been suggested earlier, the waiting time of 210 fs offers an outstanding opportunity to suppress the intramolecular vibrational contribution onto the experimental observables. First, at this time the most prominent 150 cm^{-1} mode is almost in its first recurrence (the period is ~ 220 fs). Second, by a coincidence the 485 cm^{-1} mode is in its third recurrence (the period ~ 70 fs). Third, the amplitude of the 380 cm^{-1} mode is negligibly small as compared to the other two and therefore its influence is minimized. We will use the 210 fs waiting time in a number of heterodyne-detected experiments to get rid of intramolecular vibrational involvement that masks greatly the true solvent dynamics.

Finally, the position of the maximum of the HDPE signal is displayed at two different temperatures in the Figures 6.1.e and 6.1.f. In the HDPE experiment, the echo field is heterodyned by a fourth pulse, the local oscillator [148]. By scanning the delay between the last two pulses (τ') for a set of fixed timings of the first two (τ), time resolved interferometric echo profiles are obtained. Here we focus mainly on the temporal echo amplitudes and therefore filter out the interferometric fringes by applying a Fourier-filter. For extracting information regarding the homogeneous *vs.* inhomogeneous contributions to the line broadening, the position of the echo maximum has proven to be very instructive [148]. For instance, in the framework of Bloch model, the echo maximum peaks at

$$\tau'_{\max} = \tau - \frac{\left(T_2^{inhom}\right)^2}{T_2} \tag{6.1}$$

where T_2^{inhom} and T_2 are the inhomogeneous and homogeneous phase relaxation times, respectively. If the line broadening is perfectly static, the time resolved profile peaks at $\tau' = \tau$ at all times that $\tau > 0$. At the other extreme, a totally homogeneous system produces profiles that always peak at $\tau' = 0$ fs . In the more sophisticated models of solvent dynamics [55], a relation similar to equation (6.1) also holds although the interpretation of the relaxation times becomes somewhat different [148].

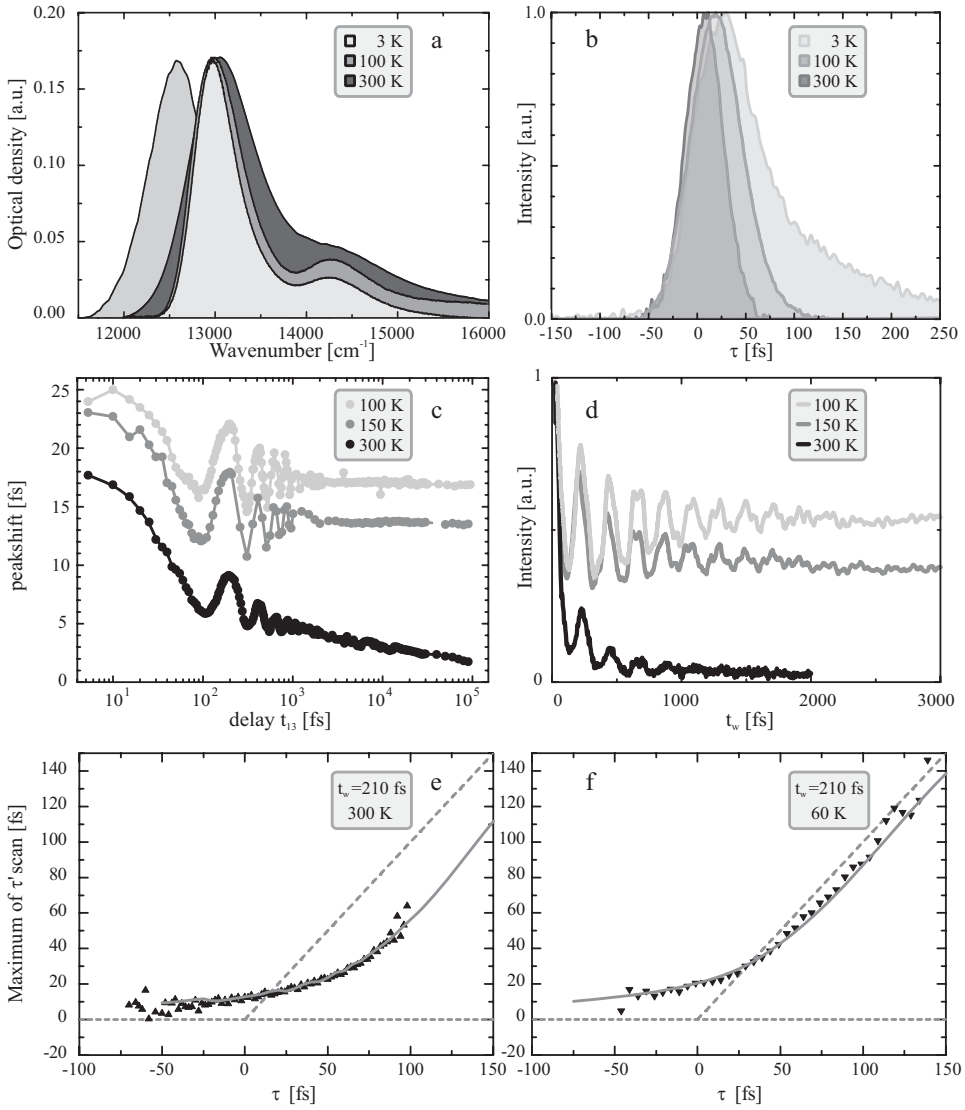

Figure 6.1. a) The absorption spectrum of DTTCI (right), and the fluorescence at 300 K (left). b) Time integrated 3PE scans for $t_{13} = 210$ fs . c) The 3PEPS signal. d) Longitudinal (t_w) 3PE scans with $\tau = 40$ fs . e) and f) The position of the transient echo maxima as a function of t_w and τ (symbols) as compared to the full scale simulations of the positions of these maxima (line) at two temperatures. The transient echo is a scan of τ ' for these specific pulse timings.

From a fleeting glance at Figures 6.1.e and 6.1.f one could conclude that the plot of the time-resolved echo maximum position obeys equation (6.1) reasonably well. From this equation one infers that the estimated dephasing time at 60 K is $T_2 \cong 60$ fs as discussed in more detail in the next sections. Furthermore, if one compares the widths and heights of these traces it becomes evident that the transient echo signal broadens with decreasing temperature, and peaks at a later time. The former corresponds to the narrowing of the absorption spectra as the temperature lowers (Figure 6.1.a) while the latter indicates their increased inhomogeneity which can not be directly deduced from the spectra. By comparing projections (i.e. integration of profiles along the τ'-axis) of both plots onto the τ-axis, the lengthening of the integrated echo signal can also be seen which is in line with Figure 6.1.b.

6.2.1 Room Temperature Data

In this section, we outline the procedures according to which different experimental data sets were processed. As a starting point, the room temperature data are used, as much is known for the dye DTTCI dissolved in ethylene glycol from the work by de Boeij [148] where 8 modes were applied to describe the dynamics. The characteristic properties of the EtOH/PD mixture are very similar to those of ethylene glycol making this choice perfect for a reference. In the next section, temperature variations of the 8 modes parameters will be introduced to explain the temperature dependent data.

All of the above experiments reflect particular aspects of the system-bath correlation function of the optical transition. For instance, the absorption and emission spectra are indicative of the overall static coupling strength parameter $\langle \Delta^2 \rangle$ and the total reorganization energy λ. The 2PE and 3PE signals are mostly susceptible to the slow parts of the correlation function. The longitudinal 3PE decay is especially useful to determine the low-frequency intramolecular modes. Alternatively, as explained in Chapter 4, the 3PEPS trace bears great resemblance to the overall correlation function, except for the shortest time-scales. This fast part of the correlation function is best determined through analysis of the time-resolved HDPE traces, as indicated above.

Therefore, all the results from all these experiments at all temperatures have to be taken into account when simulating the temperature dependence of the solute–solvent correlation function in the framework of the MBO-model. The iterative numerical procedure that is needed to calculate the correlation function and the corresponding spectral density in this manner was described earlier for DTTCI in several solvents [148-150,177,268]. It involves the simultaneous fitting of all spectra, integrated echo traces and transient echo profiles with the results from the calculations. Improvements in computer technology and optimizations

of the algorithms used in the calculations have made it possible to perform these calculations on a small cluster of 10 ordinary off-the-shelf desktop PC's.

All the calculations of the transient third-order polarization $P^{(3)}(t)$ were performed using the three-fold integrals of the complete expressions of equations (3.40) and the nonlinear response functions of equation (3.58). The actual carrier frequency and the finite pulse durations are taken into account and the measured spectral pulse profiles were used. Also, all possible pulse permutations were incorporated in the computations. After the polarization was determined, the simulated signals of the respective experiments were calculated using the appropriate expressions outlined in Chapter 3.

The contributions to the line broadening functions $g(t)$ were, depending on the nature of the mode under consideration, either evaluated directly whenever an exact expression of this function was available (see reference [145] and [148]) or through numerical integration

		Temperature:		300 K	250 K	150 K	100 K	3 K	MBO
Ultrafast mode	Gaussian decay (GCD)	$\Delta_0 = 850\ cm^{-1}$	τ_0	20 fs	30 fs	80 fs	125 fs	315 fs	no
Intramolecular modes	Vibrational modes (UBO)	$\omega_1 = 150\ cm^{-1}$	Δ_1	127 cm^{-1}	117 cm^{-1}	95 cm^{-1}	84 cm^{-1}	74 cm^{-1}	yes
		$\lambda_1 = 37\ cm^{-1}$	γ_1^{-1}	150 fs	182 fs	317 fs	317 fs	317 fs	-
		$\omega_2 = 380\ cm^{-1}$	Δ_2	43 cm^{-1}	41 cm^{-1}	37 cm^{-1}	37 cm^{-1}	36 cm^{-1}	yes
		$\lambda_2 = 3.5\ cm^{-1}$	γ_2^{-1}	500 fs	600 fs	1 ps	1 ps	1 ps	-
		$\omega_3 = 485\ cm^{-1}$	Δ_3	81 cm^{-1}	78 cm^{-1}	74 cm^{-1}	73 cm^{-1}	73 cm^{-1}	yes
		$\lambda_3 = 11\ cm^{-1}$	γ_3^{-1}	670 fs	800 fs	1.3 ps	1.3 ps	1.3 ps	-
Solvent modes	Strongly overdamped modes (SOBO)	$\lambda_5 = 20\ cm^{-1}$	Δ_5	91 cm^{-1}	83 cm^{-1}	65 cm^{-1}	65 cm^{-1}	65 cm^{-1}	yes*
			Λ_5^{-1}	0.5 ps	0.75 ps	>1 ns	>1 ns	>1 ns	-
		$\lambda_6 = 54\ cm^{-1}$	Δ_6	150 cm^{-1}	137 cm^{-1}	106 cm^{-1}	106 cm^{-1}	106 cm^{-1}	yes*
			Λ_6^{-1}	2.5 ps	3.75 ps	>1 ns	>1 ns	>1 ns	-
		$\lambda_7 = 39\ cm^{-1}$	Δ_7	128 cm^{-1}	116 cm^{-1}	90 cm^{-1}	90 cm^{-1}	90 cm^{-1}	yes*
			Λ_7^{-1}	100 ps	150 ps	>1 ns	>1 ns	>1 ns	-
		$\lambda_8 = 46\ cm^{-1}$	Δ_8	139 cm^{-1}	126 cm^{-1}	98 cm^{-1}	98 cm^{-1}	98 cm^{-1}	yes*
			Λ_8^{-1}	>1 ns	>1 ns	>1 ns	>1 ns	>1 ns	-

*Table 6.1. The temperature dependence of the fitting parameters of the harmonic modes used to simulate the optical response of DTTCI in EtOH/PD. The MBO-column indicates whether or not the temperature dependence of a particular parameter follows directly from the MBO-mode (see section 6.3 for discussion). * Only above the glass transition*

of the corresponding part of the spectral density. To do this, equations (3.55),(3.57) and (3.58) can be rewritten as:

$$\mathrm{Re}\left[g(t)\right] = \frac{1}{\pi}\int_0^\infty C(\omega)\coth\left[\frac{\hbar\omega}{2k_BT}\right]\frac{1-\cos\left[\omega t\right]}{\omega^2}d\omega \tag{6.2}$$

and

$$\mathrm{Im}\left[g(t)\right] = -\lambda t + \frac{1}{\pi}\int_0^\infty \frac{C(\omega)}{\omega^2}\sin\left[\omega t\right]d\omega\,. \tag{6.3}$$

In this way the line broadening function can be evaluated by calculating only two single integrals. At room temperature the data were simulated with the set of oscillators outlined in the corresponding column of Table 6.1.

In earlier work [148] the fastest initial decay was modelled with a quasi-continuum of undamped bath modes with a Gaussian distribution of coupling strengths (GDS, see equation (3.65)). This distribution was thought to reflect the non-rephasing coherence decay resulting from the impulsive excitation of the vibronic manifold. The fastest solvent modes were also modelled by means of a Gaussian distribution of modes that reflected the inertial solvent response, i.e. the reaction of the molecules in the first solvent shell surrounding a chromophore to the change of its electronic state and therefore the dipole moment. The Gaussian character of this GDS profile is supported in liquids by molecular dynamics simu-

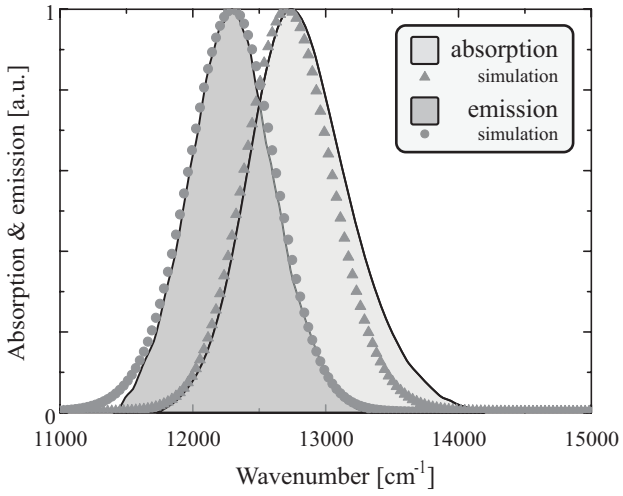

Figure 6.2. Absorption and emission spectra at 300K and the results of the corresponding simulations. The absorption due to ring modes at 14000 cm^{-1} has been subtracted from the overall spectrum (see text for details).

lations and optical response theory [121-124,129,271,272] and also by optical Kerr and Raman data on similar neat solvents [149,273-278]. In polymers it was suggested that this solvent response was best fitted by a critically damped oscillator [150].

For reasons that are discussed in the following sections and that follow from the temperature dependence of the ultrafast components of the correlation decay, both the fast intramolecular mode and the inertial solvent mode are modelled by a single decay of the correlation function, in the simulations performed here. This decay is taken to have a Gaussian shape centred at $t = 0$:

$$M(t) = \frac{\Delta_0^2}{\tau_0} \exp\left[\frac{-t^2}{\tau_0^2}\right]. \tag{6.4}$$

This Gaussian correlation decay (GCD) is associated with the following expression for the corresponding spectral density $C(\omega)$:

$$C(\omega) = \frac{\Delta_0^2 \lambda \omega}{\sqrt{\pi}} \exp\left[\frac{-\omega^2 \tau_0^2}{4}\right]. \tag{6.5}$$

The shape of the contribution of this mode to the overall SD is shown in Figure 6.14.b.

Besides these fast components to the correlation function, the optical transition of DTTCI is coupled to three distinct intramolecular vibrational modes modelled with under-

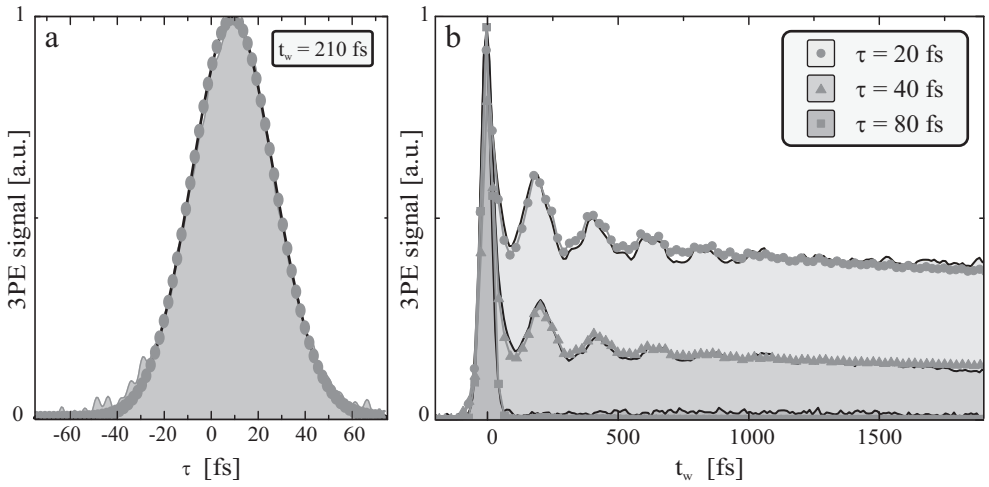

Figure 6.3. a) A typical 3PE trace as used in the determination of the 3PEPS at 300 K. The grey dots show the simulated echo trace. b) The longitudinal 3PE at three coherence times τ at room temperature. Again, grey black symbols show the simulations of these experiments.

damped Brownian oscillators (UBO's, see equation (3.63)). These modes model the periodical recurrences of the observed optical coherence.

After the ultrafast initial decay, and somewhat masked by the quantum beats due to the slow vibrational modes, solvent motions make the correlation function decay further on two picosecond time scales. This is in line with previous experiments, and this part of the decay is modelled by means of strongly overdamped Brownian oscillator (SOBO, see equation (3.69)). It is attributed to diffusional solvent motions. A final SOBO with a decay time set to infinity (≥ 1 ns) was used to model the residual inhomogeneity that was invariably found in the response of viscous liquids.

Figures 6.2 through 6.8 outline the results of simulations using the above parameters and expressions. It shows that the set of parameters from Table 6.1 can be used to describe all room temperature experiments adequately.

Figure 6.2 displays the emission and absorption spectra at room temperature. Note that the part of the DTTCI absorption spectrum that is due to excited modes of the conjugated rings of the dye has been largely subtracted to facilitate the comparison of the experimental and simulated data. This was done by fitting these modes on the blue side of 14000 cm^{-1} with a single Gaussian and subtracting the resulting fit

The calculated spectra fit the data very well, except for the small offset on the red side of the emission spectrum. This is more often observed in simulations of the linear spectra with the MBO-model. The limited number of modes explicitly considered in the model causes the vibronic coupling to be easily underestimated. In addition, the harmonic model does not

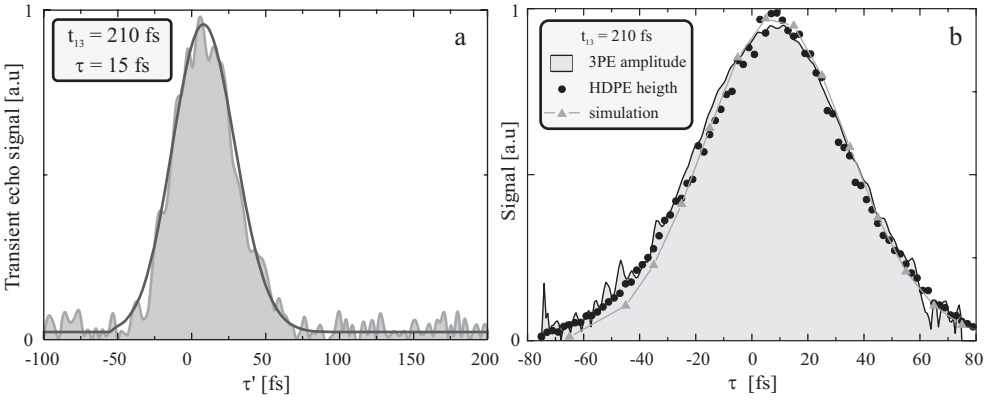

Figure 6.4.a) A typical filtered HDPE trace at room temperature and the corresponding simulated transient echo trace. b) A comparison of the amplitude of the 3PE with the height of HDPE traces and the transient echo simulations.

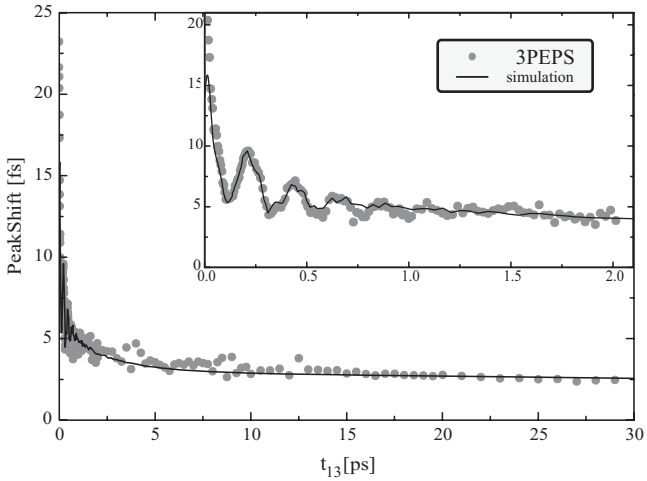

Figure 6.5. The 3PEPS signal of DTTCI in PD-EtOH at room temperature and the calculated peakshift trace. The insert shows the short waiting time data.

include any difference between the potential energy surfaces of the ground and excited state of DTTCI. This could be the case as suggested by the fact that emission and absorption are not perfect mirror images. If these surfaces are not identical, the energy gap is no longer linearly coupled to the generalized solvation coordinate, and quadratic coupling terms need to be considered as well. This leads to extra dephasing terms that should be taken into account. Possible anharmonicity of the potential energy surfaces is a related process that leads to the appearance of the nonlinear coupling. However, this is less likely to be important at room temperature because at this temperature the fast bath dynamics ensure the Gaussian statistics of the fluctuations of the energy gap. At temperatures below the glass transition the bath dynamics become far more static, and therefore the particle averaging of the solvent motions might be less effective. Then the Gaussian character of the statistics of the collective solvent coordinate is less probable

Besides reproducing the absorption and emission spectra, the same parameter set also reproduces the 3PE traces as shown in Figure 6.3. The simulations of longitudinal 3PE profiles show that the quantum beats that are modelled by the three UBO's, are reproduced perfectly. This is demonstrated in Figure 6.3.b. These same recurrences are also observable in the 3PEPS signal, demonstrated in Figure 6.5. The traces are reproduced as well in the calculations, except for the shortest waiting times, as was to be expected.

Next, the 3PE signal is time-resolved using a local-oscillator pulse in the HDPE experiment. A typical time-resolved trace and the corresponding prediction are shown in Figure

6.4.a. To demonstrate the comparative merits of these transient echo traces with the time-integrated 3PE signal, the maximum heights of the HDPE curves is plotted against the amplitude of the 3PE. Figure 6.4.b. shows that the square root of the time-integrated signal matches the heights of the transient echoes.

After having established the relation between the 3PEPS and the HDPE experiments, Figure 6.6 shows the full HDPE plots for several waiting times. Although it is possible to discern some increase in the homogeneous character of the time-resolved echo profile and coherence loss with increasing τ', these 2D plots are not very instructive when analyzing the correlation functions or the system – bath spectral density. The time-resolved echo at $t_w = 210$ fs has an ellipse shape, stretching to some extent along the $\tau' = \tau$ axis. The echo signal at $t_w = 100$ ps has a more circular shape, stretching more along the $\tau' = 0$ direction.

In order to quantify these findings, in Figure 6.7.a the same data as in the top left panel of Figure 6.6 is shown, but now with all τ'-traces are normalized. This illustrates the development of the position of the transient echo maximum along the τ-axis. In the subsequent panels of Figure 6.7 the position of the maximum of a fit of the transients with a Gaussian profile is plotted. These maxima are useful when interpreting the behaviour of the HDPE signal with varying waiting time and temperature.

The position of the maximum can be interpreted in terms of equation (6.1) as also outlined in Section 3.7. For the moment however, the positions of the maxima are only compared to those of the calculated transient echo traces in order to once more ascertain that the parameter set from Table 6.1 describes both the fast and slow parts of the correlation functions satisfactorily at room temperature. It is immediately clear form the five latter panels of Figure 6.7 that this is indeed the case; the calculations match the experimental data closely. Figure 6.8, that shows the variation of the maximum position with the waiting time for several coherence times, confirms this.

This shows that all experiments and data sets at this temperature can be reproduced with the parameter set of Table 6.1. At first sight an optimization space spanned by nearly 30 free parameters might seem rather excessive. However it is important to realize that not all these factors are free to take any value. The amplitude Δ_i of each mode is related the reorganization energy λ_i associated with that mode through the equations outlined in section 3.6.2.

Although adding more BO modes would of course improve the agreement between experiment and simulation, it is not possible to describe the data accurately with fewer oscillators. The fast initial 3PEPS decay shows clear evidence of two components, and the longitudinal echo traces necessitate the use of at least three UBO's. The diffusive solvent modes are determined by four SOBO's. Residual inhomogeneity and the 3PEPS decay at waiting times over 1 ps clearly show why the three slowest modes need to be considered.

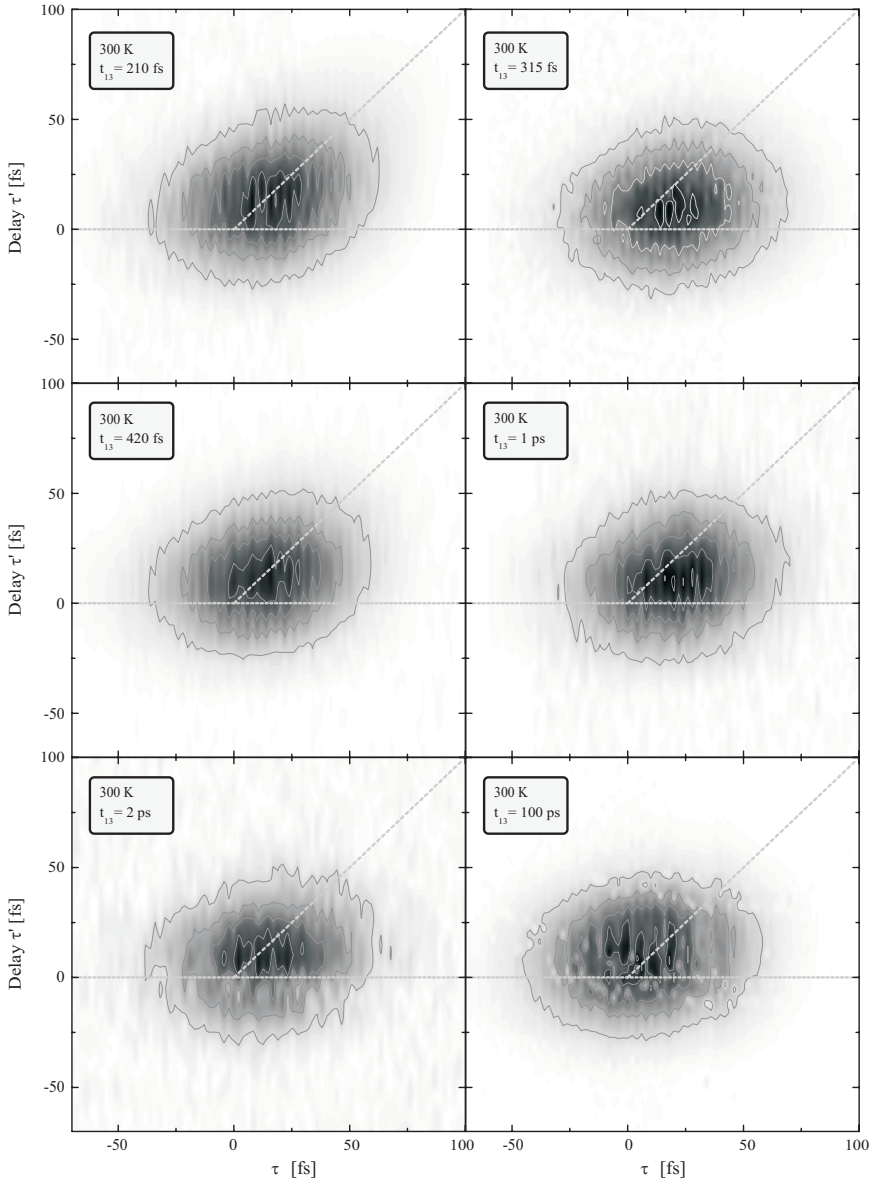

Figure 6.6. 2D representations of the HDPE scans at four different waiting times. The dashed lines are $t_{34} = 0$ *fs and* $t_{34} = \tau$ *and indicate the position of the maxima of the transient echo traces in the case of perfect homogeneous and completely static line broadening respectively.*

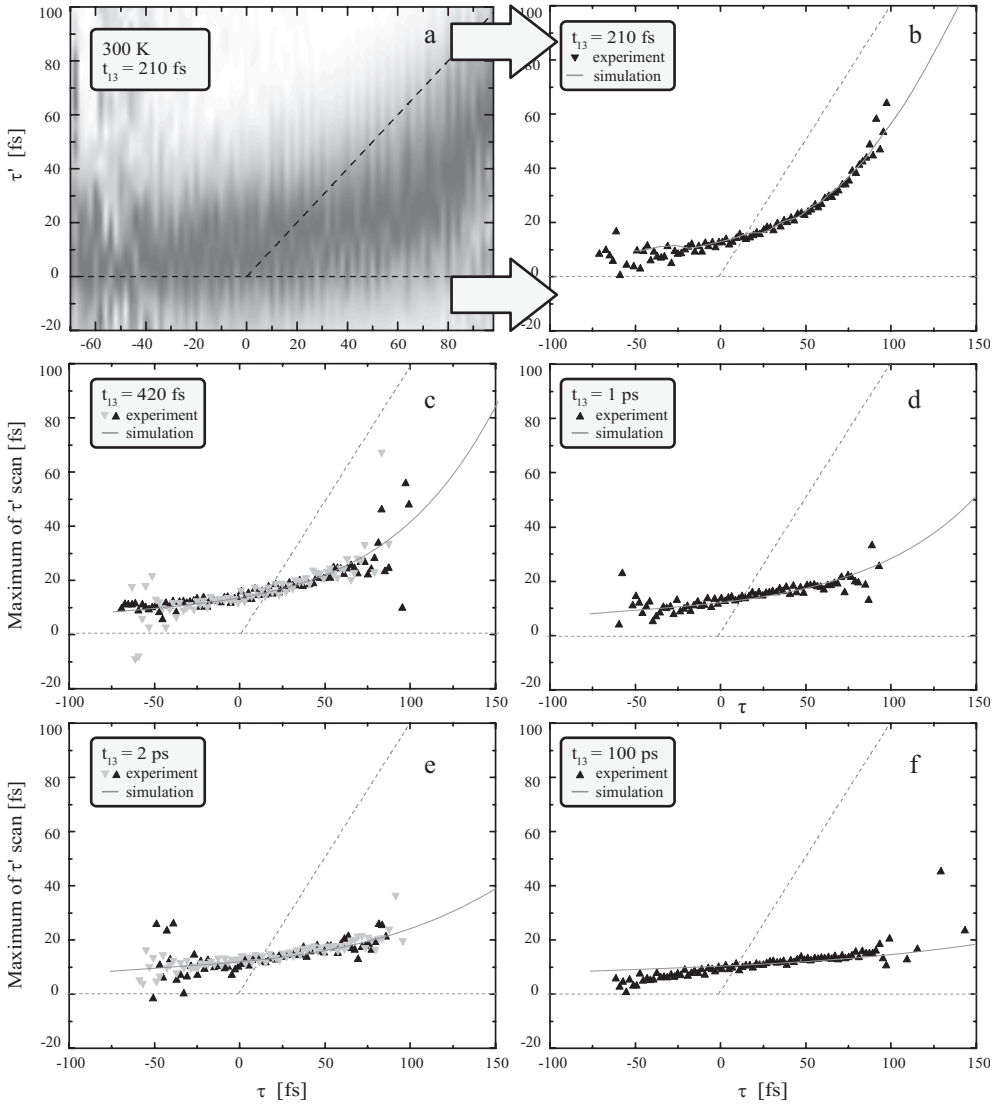

Figure 6.7.a) The HDPE plot as in Figure 6.6 with t_{13} = 210 fs and all traces along the t_{34} axis normalized. b) – f) The position of the maxima of the transient echo traces for several waiting times at room temperature (symbols) and the corresponding results of the calculations (lines).

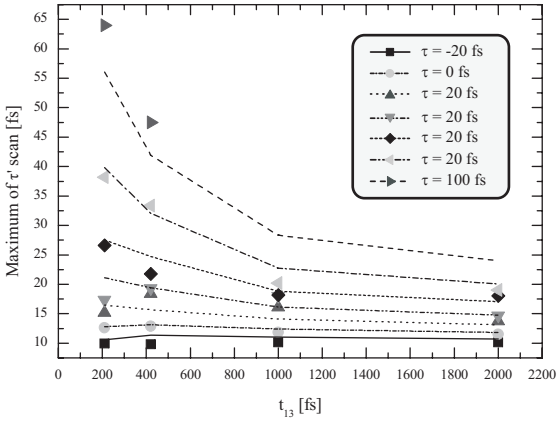

Figure 6.8. The dependence of the position of the maximum of the transient echo traces for several coherence times τ (symbols) and the corresponding theoretical predictions (lines).

The 500 fs mode is not as obvious since it is somewhat masked by the quantum beats due to the vibrational modes, but fits to the 3PEPS signal and longitudinal echo traces clearly improve when this mode is added to the simulations.

Now that the room temperature data are described adequately by the current set of BO's, it is time to verify how these oscillators can be used to described the data after a temperature change.

6.2.2 Temperature Dependent Data

The spectral density of states is the key quantity in modeling the system – bath interactions. In a first approach it is supposed not to be dependent on temperature. Even if one considers a temperature independent spectral density as a starting point for these calculations, some temperature effects still can be incorporated in the MBO-model through the Boltzmann term in equation (6.2). On the same footing the parameters of the different types of modes depend on temperature. For an UBO e.g. the amplitude of the oscillations can be calculated from the associated reorganization energy and the temperature as follows:

$$\Delta_i^2 = \lambda \omega_i \coth\left[\frac{\hbar\omega_i}{2k_B T}\right]. \tag{6.6}$$

When the so-called high temperature limit (HTL) holds, i.e. when the frequency of the mode is low enough with respect to the temperature as in $\hbar\omega_i \ll 2k_BT$, this reduces to

$$\Delta_i^2 = \frac{2k_BT\lambda_i}{\hbar}. \tag{6.7}$$

This second expression for the amplitude of the frequency excursions is also valid for a SOBO in the HTL when the nuclear dynamics of the mode in question are slow compared to the magnitude of the fluctuations ($\Lambda_i \ll \Delta_i$). These temperature dependencies get expressed in the correlation functions $M'(t)$ and $M''(t)$ through the line broadening function $g(t)$, see equations (3.56), (3.57) and (3.58).

It should be noted that the modes included in the spectral distribution associated with the GCD cannot suit the HTL. At room temperature modes faster then $\sim$15 fs do not satisfy this limit. At 30 K the HTL no longer holds for modes faster then ~150 fs and at 3 K even the quickest diffusional mode might not meet the constraints of the HTL.

Even if the 300 K parameter set is considered to describe a temperature independent spectral density, the model can accommodate temperature variations. However, it is not likely that the SD remains unchanged over the whole temperature range from 300 to 3 K, especially since this range includes a phase transition.

Close inspection of all the outcomes of all experiments at various temperatures, as sum-

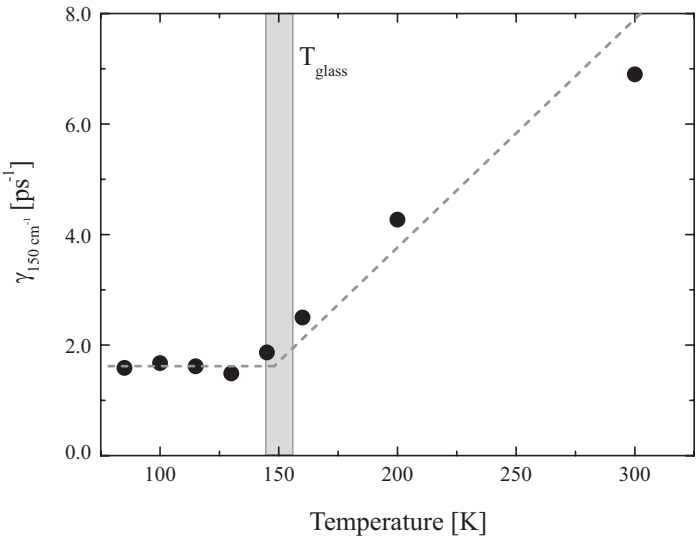

Figure 6.9. The temperature dependence of the damping of the 150 cm^{-1} vibrational mode of DTTCI in EtOH/Pd shows the effect of the glass transition (grey bar) on the vibrational mode.

marized in Figure 6.1, shows that the most apparent temperature dependent feature is the damping constant of the UBO's as seen in longitudinal echo decays and 3PEPS plots. When the longitudinal 3PE plots are fitted with the damping factors γ_i as free ranging parameters, the behavior of especially the damping of the 150 cm^{-1} mode shows a significant temperature dependence. This dependence is plotted in Figure 6.9. Below the glass transition temperature the slowing of the damping of this mode stops. In fact, this slowing of the damping of the intramolecular vibrational modes is the most straightforward observation of the glass transition upon inspection of the individual experiments.

However, for a proper analysis, evaluating all the experiments one by one will not do. What is needed, is a scenario that can explain all experiments within the confines of the MBO model. The above example does show it is not possible to describe all data with a completely temperature independent SD. Consequently, some additional temperature dependence of the SD needs to be incorporated in a model that makes physical sense, while varying as few BO parameters as little as possible.

In the following, the outcomes of several experiments are presented at several temperatures. In order to establish the need for a SD that depends on the temperature, some of these experiments are compared both to calculations that were based on a temperature independent SD and to calculations that include a SD that changes with temperature according to a single set scenario.

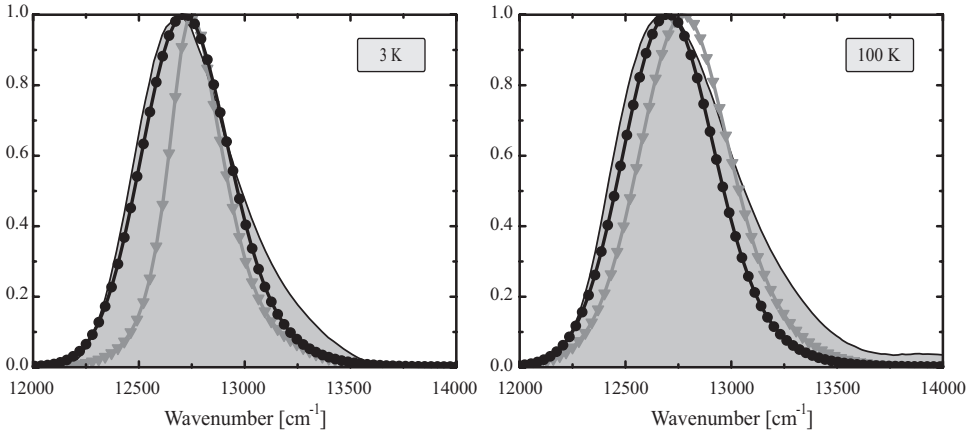

Figure 6.10. The absorption spectra of DTTCI in EtOH/PD at two different temperatures and the calculations of these spectra with the parameters in Table 6.1 (black circles). To emphasize the need for a temperature dependent SD to accurately simulate the data, the grey triangles indicate the absorption spectrum simulated with a temperature independent SD that was deduced from the room temperature data.

After having tried many possible scenarios, the data were successfully simulated with a spectral density that is still nearly temperature independent. The conjecture was a scheme in which all the intramolecular modes were supposed to show the temperature dependence through the relations within the MBO model as outlined above. Only the dissipation of vibrational energy into the surroundings is sensitive to the temperature. From Figure 6.9 the following relation was inferred:

$$\gamma_i = \begin{cases} \alpha\gamma_{room}\dfrac{T-T_g}{T_{room}-T_g} + (1-\alpha)\gamma_{room} & \text{for } T \geq T_g, \\ (1-\alpha)\gamma_{room} & \text{for } T < T_g. \end{cases} \tag{6.8}$$

Here γ_{room} is the value of γ_i at room temperature T_{room} and $0 < \alpha < 1$. At the glass point the friction is typically halved with respect to room temperature ($\alpha \cong \frac{1}{2}$), and becomes temperature independent below T_g. It is reasonable to assume that when the bath dynamics slow down, the vibrational energy of the chromophore dissipates slower. However, the

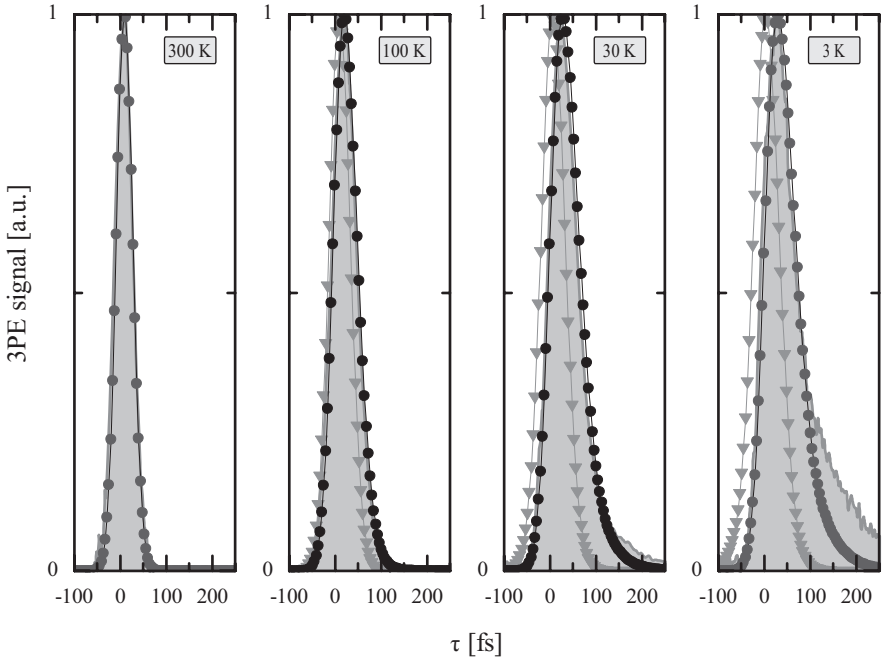

Figure 6.11. An example of typical 3PE traces at various temperatures. The waiting time for these traces is $t_{13} = 210$ fs. The black circles indicate the simulations with a temperature dependent SD and the grey triangles simulations with a temperature independent SD.

choice for a linear temperature dependence and a damping factor below the glass transition that is half the room temperature value is made on phenomenological grounds.

At the same time, when considering the solvent modes, it makes sense to expect that all diffusion vanishes at the glass temperature. Therefore, a temperature dependence was introduced for SOBO's, that confirms with the freezing out of solvent diffusional modes. The strongly overdamped solvent modes were considered as contributing to the overall static inhomogeneity below the phase transition. The data were adequately described at all temperatures below T_g by setting the parameters of the *i*-th SOBO as follows: the correlation time Λ_i^{-1} was set to infinity (>1 ns) and Δ_i^2 was set to its value at the glass temperature according to equation (6.7). Above the glass temperature Λ_j was set to linearly increase from zero to its value at room temperature:

$$\Lambda_i = \Lambda_{room} \frac{T - T_g}{T_{room} - T_g} . \tag{6.9}$$

This proposed behavior is inspired by the Vogel-Fulcher equation [27,28] describing non-Arrhenius relaxation in glass forming liquids, see equation (2.3). Here the divergence temperature in the argument of the exponent in equation (3.68) is set equal to the glass temperature. Δ_i^2 was set according to equation (6.7) above the glass point.

So far, this scenario is simple and physically appealing, since it only implies the slowing down of solvent modes and vibrational energy dissipation as the glass transition is approached. Unfortunately, it yields too little inhomogeneity which results in a peakshift that

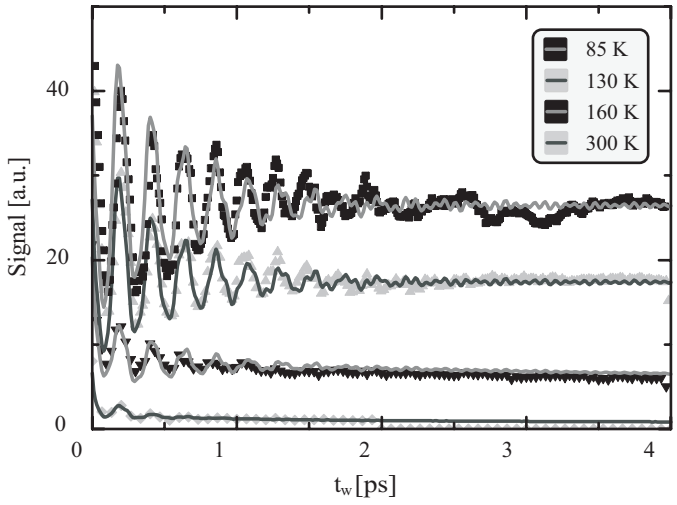

Figure 6.12. The longitudinal 3PE traces with $\tau = 40$ fs at several temperatures (symbols) and the corresponding calculations (lines) according to Table 6.1.

is too small at temperatures well below T_g. If the 3PEPS traces are calculated using the above scenario with a fast mode as in section 6.2.1., where the contribution of the fast mode only varies with temperature through the standard MBO relations as in equation (6.2) and (6.3), the traces do not match the experimental data. In this case the simulated data differ from the experimental data with an off-set that is constant at all but the fastest waiting times for a set temperature. For instance, Figure 6.14.a shows the difference between the calculated 3PEPS using the parameter temperature variation as introduced above and the experimental 3PEPS data at several waiting times as a function of temperature. The parameters of the fast mode were set to match the data at room temperature. Clearly an off-set exists between the calculated peak-shift and its experimental value which is virtually identical at all waiting times and which varies nearly linearly with temperature. This indicates that the fast MBO-modes must also vary with temperature.

De Boeij *et al.* used two Gaussian distributions of spectral modes (GSD) to describe the ultrafast part of the correlation decay [148,171,268]. If the parameters that are used to describe these distributions are taken to be temperature independent the data, of course, cannot be accounted for. As indicated, in this case the 3PE traces peak to early and the simulated data have an excessive homogeneous character. Of course this can be fixed by making the parameters of these two GSD's that de Boeij *et al.* used temperature dependent. In such a way the influence of the ultrafast part of the simulated correlation decay can be decreased at lower temperatures. Unfortunately, doing so will yield 3PE decays with unrealistically long tails, or in other words simulated echo decays that stretch to far longer times than the experimental data. Fitting both experiments with one parameter set seems impossible with

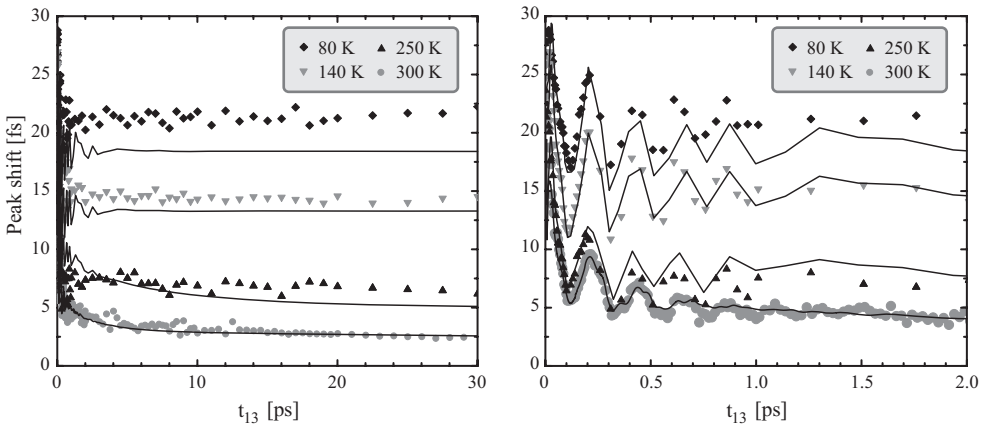

Figure 6.13. Temperature dependent 3PEPS data (symbols) and the corresponding simulations according to the scenario as outlined in the text (lines).

this GSD-type of ultrafast modes.

For this reason the Gaussian decay of the correlation function (GCD) was introduced in the previous section. This is the decay as described by equation (6.4). It differs only slightly from the GSD mode; the amplitude of the Gaussian correlation decay is divided by τ_0. By increasing the characteristic timescale τ_0 of this mode with decreasing temperature the ultrafast decay was slowed enough to let the simulated 3PE traces peak at a time that corresponds with the experimental 3PEPS data while at the same time it still had enough amplitude to yield realistic simulated 3PE data. Therefore both the solvent and the intramolecular GSD were replaced by this single GCD in the simulations.

The temperature dependence of the characteristic time of the GCD was chosen to be exponential. Since the 3PEPS does not vary linearly with the amplitude of this mode, a simple linear temperature dependence of τ_0 could not explain the experimental results in a satisfactorily manner. Other non-linear functional forms of this dependence can also be used. The exponential form was chosen for its simplicity only, and it yields a temperature dependence of τ_0 that goes as:

$$\tau_0 = \alpha_1 \exp\left[\frac{-T}{\alpha_0}\right]. \tag{6.10}$$

The values of τ_0 that were used in the calculations are listed in Table 6.1 and are also

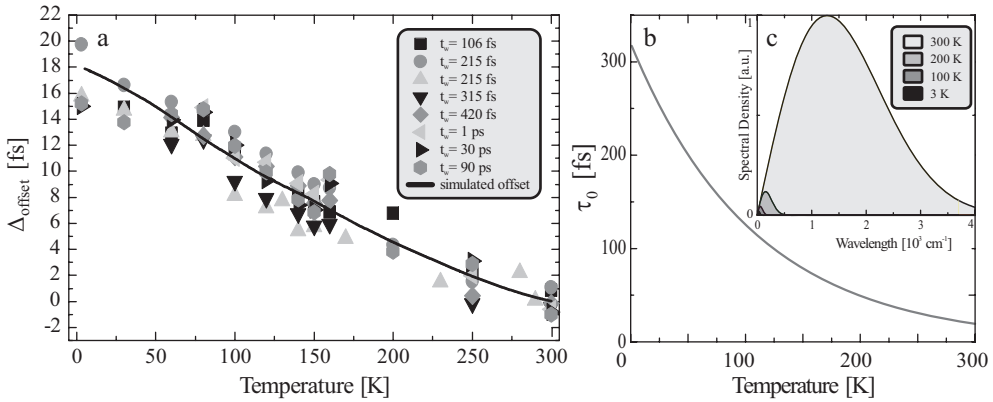

Figure 6.14. a) The difference between the experimental data at several waiting times and the simulated 3PEPS data without considering the temperature dependence of the fast GCD mode (symbols, see text). The solid line shows the difference between the simulation with and without this temperature dependence. b) The temperature dependence of the characteristic time τ_0 of the GCD mode used in this calculation. c) The spectral density associated with this temperature dependent GCD-mode.

shown in Figure 6.14.b. These values were obtained by setting $\alpha_0 = 107$ K and $\alpha_1 = 320$ fs. The amplitude Δ_0 of the mode was taken to be temperature independent. Since at all temperatures the characteristic times is still shorter than all the other modes this effectively means that the amplitude of the fast mode varies as $\propto \Delta^2/\tau_0$. In principle, other parameterization functions, for instance, involving both parameters, could have been used as well. The difference between the simulated peak-shift data without the temperature dependence of this fast mode and with a fast mode that varies as in equation (6.10), is represented by the solid line in Figure 6.14.a. This shows that the chosen dependence for this mode is effective in eliminating the last remaining difference between the simulated 3PEPS traces and the experimental data.

The temperature dependence of this particular SD change is depicted in the inset of Figure 6.14. Although its temperature variations are not as physically appealing as those of the modes introduced earlier in this section, the overall behaviour does make perfect sense. With the temperature decrease, the SD of the bath fluctuations, in the first place, spans a narrower spectral region, and secondly, decreases in amplitude. As the fast intramolecular mode is usually associated with fast vibrational dephasing, both trends meet the intuitive expectations. However, the observed temperature dependence does not follow automatically from the MBO model, most probably, due to the breakdown of the assumption of lin-

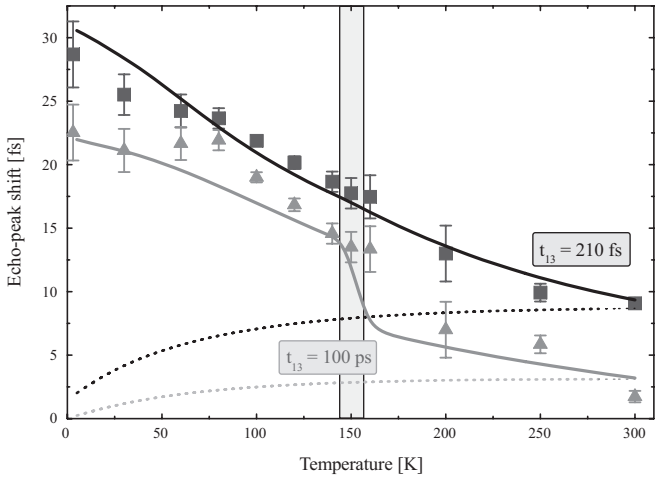

Figure 6.15. The temperature dependence of the echo peakshift at waiting times t_{13} = 210 fs (black) and t_{13} = 100 ps (grey). The glass temperature T_g is indicated by the grey bar. The solid lines are simulations of the experimental data using the scenario outlined in the text. The dotted lines are simulations of the 3PEPS experiment assuming a fixed, temperature independent, SD.

ear coupling to the vibronic manifold.

After this final tweak the scenario yields good results. Of course having more parameters vary more freely with temperature can improve the match between experimental results and the calculations, but this scenario is of all tested arrangements the simplest one that can describe the results adequately.

The first evidence of the ability of this scenario to describe the data is with the temperature dependence of the absorption spectra. This is presented in Figure 6.10. In all absorption spectra the ring modes with a 16000 cm^{-1} detuning were subtracted. This was done by fitting this part of the spectrum with a Gaussian profile and subtracting the resulting fit. The spectra can be accurately reproduced over the complete temperature range. All relevant parameters are also outlined in Table 6.1.

The 3PE echo profiles as reproduced similarly well at all waiting times and temperatures except for short waiting times (< 1 ps) at very low temperatures (< 5 K). Since at these times and temperatures the HTL no longer holds, the mismatch between experiment and simulation in the last panel of Figure 6.11, was to be expected. Otherwise the echo width and echo position are reproduced exactly. Also the longitudinal echo traces are reproduced, as demonstrated in Figure 6.12.

Especially the longitudinal echo traces reinforce the necessity of making the damping of the vibrational modes temperature dependent. The temperature dependence of the parameters that make up the UBO modes is characterized accurately. Close inspection shows that although there is some room for improvement of the fits, the data do not yield evidence enough for more complicated schemes than the one described in equation (6.8).

Figure 6.13 also shows the effectiveness of the proposed scenario. The 3PEPS data are reproduced reasonably well at the various temperatures. It shows evidence of the separation in the fast intramolecular modes not being sensitive to the glass transition and the diffusive solvent modes that are susceptible to this phase transition. Although at some temperatures the experimental asymptotic long time peakshift is not perfectly reproduced in the simulations, the trends of the values are replicated quite well. The mismatch between experiment and simulations is too small to warrant further refinement of the proposed temperature dependence.

The next plot perhaps best demonstrates this. Figure 6.15 plots the detailed temperature dependent data of the 3PEPS at two waiting times that correspond to the first vibrational recurrence at 210 fs and almost full relaxation at room temperature at 100 ps. The temperature dependence of these peaks shifts is correctly emulated by the simulations. The short time peakshift shows little evidence of a discontinuity at the phase transition. This is reasonable to expect, since the fast modes are not sensitive to this change in the bath dynamics, and the solvent modes are too slow to influence the peakshift at this waiting time.

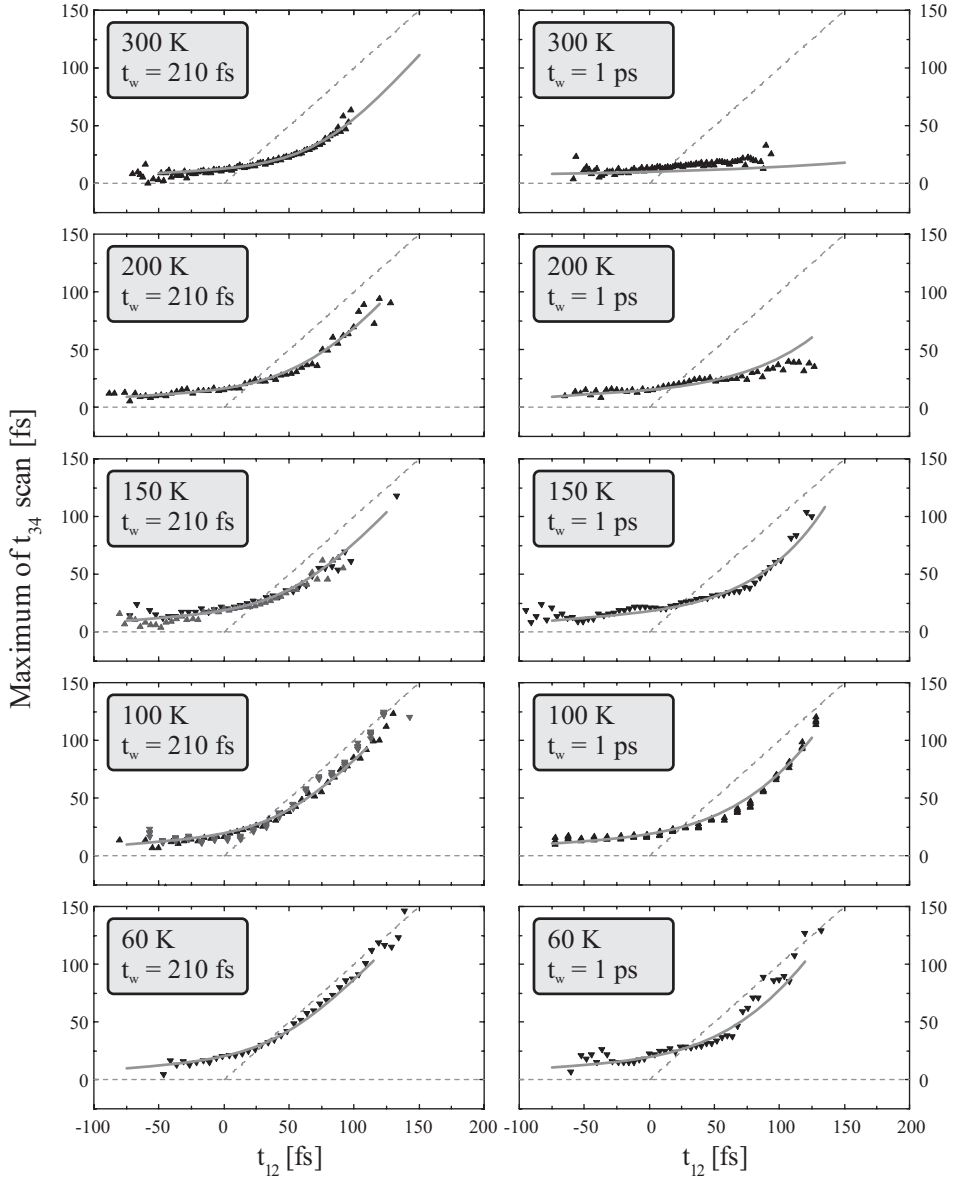

Figure 6.16. The maxima of transient echo traces at various temperatures and two waiting times (black and grey triangles) with the corresponding calculations (grey lines). The dotted lines are guides for the eye as in Figure 6.7.

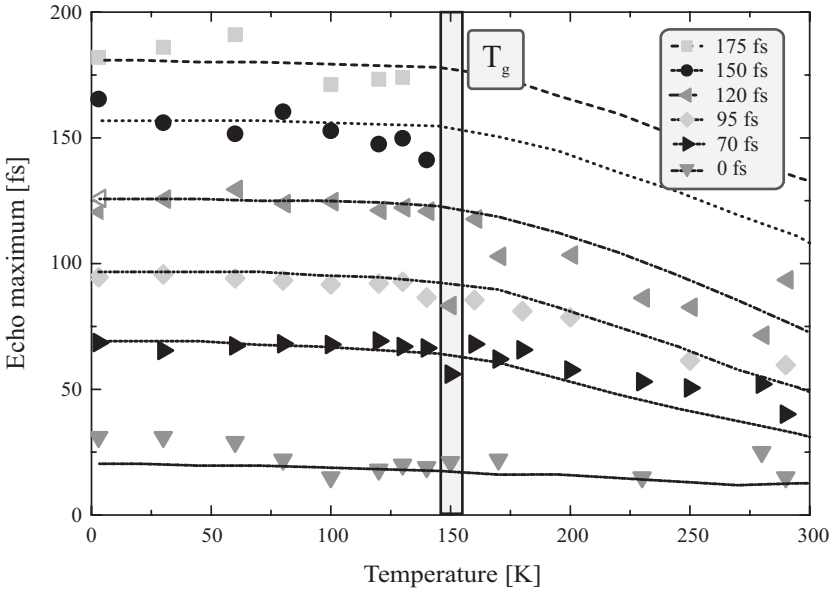

Figure 6.17. The position of the maximum of the time resolved echo profile at different coherence times τ as a function of temperature and the corresponding calculations. The waiting time was set at 210 fs.

Only at long waiting times the glass to liquid transition is visible in the experimental 3PEPS results. At even lower temperatures, as the system becomes more inhomogeneous, the solvent relaxation nearly vanishes altogether. The offset between these two data sets at temperatures below the glass transition, therefore originates mainly from the vibrational relaxation of the 150 cm^{-1} intramolecular mode and the temperature dependent terms in equation (6.2).

Finally, the temperature dependence of the HDPE data is demonstrated in Figure 6.16. Comparing this figure with Figure 6.7 shows that the shape of the echo profiles is clearly changed with the temperature decrease. Actually, decreasing temperature and decreasing waiting time have a similar effect on the shape of the 2D plots, it makes them more asymmetric. This asymmetry is an indication of a more inhomogeneous character of the frequency fluctuations. As with the room temperature data, the maxima of the Gaussian fits to the transient echo traces are plotted as a function of the coherence time. These maxima positions of the maxima also compare well with the theoretical predictions based on the proposed scenario.

Figure 6.17 shows the temperature dependence of the maximum of several slices of these echo maximum profiles at different temperatures and at a waiting time of $t_w = 210$ fs . It is immediately clear that the system grows to be more static at lower temperatures. From 300 K to the glass temperature at 150 K, the dynamics slow down in a linear fashion. Then, deceleration of the solvent dynamics seemingly comes to a halt around the glass temperature.

The glass transition is clearly discernable in the experimental HDPE data even at this waiting time, as opposed to the temperature dependent 3PEPS data. At longer coherence times at low temperatures the maxima are positioned at nearly the same delay as the corresponding coherence time, indicating a purely static and inhomogeneous character of the dephasing dynamics. The HDPE data are well reproduced by the proposed scenario for the temperature dependence of the BO parameters.

6.3 Discussion

The scenario for the temperature dependence of the spectral density discussed and investigated in the previous section can be used to successfully simulate the experimental data. The choices implemented in this scenario are made on phenomenological grounds. The feasibility and credibility of these grounds are discussed in further detail in this section.

Within the MBO model and still assuming a temperature independent shape of the spectral density, the amplitude of the frequency fluctuations Δ_i are assumed to depend on temperature while the associated reorganization energy λ_i is a constant instead of the other way around. The justification of this assumption lies in the fact that in the framework of the MBO model the reorganization energy is directly connected with the displacement d between the ground and excited state potential energy surfaces of the chromophores along the generalized solvent coordinate. Also, the absorption spectra exhibit some narrowing of their widths at lower temperatures which is consistent with decreasing of the frequency fluctuations. Finally, the argument that the Stokes shift (that is directly related to the reorganization energy) decreases with decreasing temperature, is refuted by noticing that the time scale at which the solvent reorganization occurs, at low temperatures becomes much longer than the excited-state lifetime. Therefore, the population relaxes long before the solvent has a chance to get reorganized.

The temperature dependence of BO parameters (i.e., reorganization energy λ_i , damping γ_i and frequency ω_i) is rarely discussed in current literature on harmonic oscillator solvent models. Gu *et al.* [279] remark, in their full quantum mechanical treatment of an electronic excitation linearly coupled to multiple passively damped harmonic oscillators, that in

a general approach the damping coefficient should be regarded as a function of temperature and frequency $\gamma_i = \gamma_i(T, \omega)$. They note that the specific temperature dependence is especially relevant if one considers the effects of a phase transition of the solvent. The ultimate cause of the damping of the UBO modes is the interaction of the optical system with the environmental solvent shells, and one would expect a large effect on the damping from the fluid viscosity. Therefore the authors conclude that the temperature dependence of γ_i is determined by the specific physical origin of the damping of the mode under consideration.

For these reasons in the last column of Table 6.1 the parameters that vary with temperature purely following equations (6.6) and (6.7) are indicated as following directly from the MBO model, whereas the temperature dependence of the damping parameters γ_i and Λ_i is not included in the model. This dependence was chosen in such a way that the simulations fit the experimental data.

The damping of the slow intramolecular modes discussed here, is determined by how quickly the vibrational energy dissipates into the surrounding solvent. In the absence of a solid theoretical framework the choice for linear variation of the damping of the underdamped oscillator with temperature follows readily from the experimental longitudinal 3PE data, as can be seen in Figure 6.12. The damping rates are relatively small, the decay rates of the oscillations are on the subpicosecond time scale. The slower relaxation processes, related to structural equilibration, should correlate well with the Stokes-Einstein equation that provides the relation between the self-diffusion coefficient D and the viscosity η:

$$D(\eta) = \frac{kT}{6\pi\eta r} \tag{6.11}$$

As pointed out in section 2.1, a similar relation exists for the rotational reorientation time, the Debye–Einstein relation. Therefore, as the diffusion coefficient decreases linearly with temperature, the microscopic structural relaxation times will increases in a similar fashion. It has been established [280,281] that this concept of evaluating hydrodynamic and thermodynamic functions of the solvent can be used to describe the solute oscillator – solvent coupling. The linear character of temperature dependence has been observed in Raman spectra of amorphous metal solids [282] and in IR pump-probe studies on the temperature dependent vibrational relaxation times of carbonyls solutes in various liquids [283,284]. Although this evidence is indirect, it indicates that the linear temperature dependence of the vibrational relaxation in the experiments presented here is reasonably realistic.

The temperature dependence of the inverse correlation time Λ_i of the strongly overdamped modes is established using the same concept of correlated temperature dependences of relaxation times. As it is reasonable to expect that all diffusive motion disappears at temperatures below the glass transition, this temperature is used as the divergence temperature in a Vogel-Fulcher description [27,28]. As outlined in section 2.1, this is a first-

order approach to model non-Arrhenius relaxation in glass forming liquids. Transient-dichroism experiments however, have demonstrated a similar correlation with viscosity and temperature [285-293].

The main experimental motivation for the linear temperature dependence of the inverse correlation time Λ_i of the solvent modes above the glass temperature was the temperature dependence of the HDPE traces, as displayed in Figure 6.17. This can be easily understood by examining the transient echo signal. This signal follows the following relation:

$$S_{HDPE}\left(\tau, t_w, \tau'\right) \propto \left|P^{(3)}_{3PE}\left(\tau, t_w, \tau'\right)\right|^2 \tag{6.12}$$

Differentiating this for a polarization determined by some correlation function $M'(t)$ made up of a fast part $M'_{fast}\left(t_{23}\right)$ and some slow SOBO modes contributing to $M'_{slow}\left(t_{23}\right)$, as in

$$M'(t) = (1-a)M'_{fast}(t) + a\,M'_{slow}(t)\,, \tag{6.13}$$

will yield its maximum position $t_{\max}$ as was shown in section 3.7. At long coherence times this gives for the maximum position:

$$\left(\frac{\partial t_{\max}}{\partial \tau}\right) = M'_{slow}\left(t_w\right). \tag{6.14}$$

And therefore, in a first order approximation, the linear dependence of the maximum position on the inverse correlation time can be expressed as:

$$t_{\max} = \tau - \frac{\Lambda_i}{\Delta_i^2}\,. \tag{6.15}$$

This shows that any other but a linear temperature dependence of the diffusive solvent mode parameters does not lead to an adequate description of the experimental results. It also reinforces the connection between the 3PEPS and the HDPE results, as changing the parameters of the strongly-overdamped modes to match, for instance, the peakshift data will also change the transient echo maximum position.

Whereas the temperature dependence of the parameters of the above modes are in accordance with the physical interpretation of the associated relaxation processes, the temperature dependence of the amplitude of the fastest intramolecular GCD mode does not follow naturally from the interpretation that this mode arises from ultrafast dephasing of the vibronic manifold. In studies of liquid dynamics in the femtosecond time domain, the solvent relaxation decays are divided into slow diffusive components and a fast inertial contribution. The latter component is not necessarily viscosity dependent. Here the amplitude of the ultrafast GCD of the correlation function was taken to vary exponentially with temperature through the characteristic time τ_0. This functional dependence was chosen on purely phenomenological grounds and also for its simplicity. However the experimental data can also be described with other non-linear functional dependencies with sufficient accuracy.

Summarizing the discussion on the temperature dependent parameters, all the BO parameters that vary with temperature, do so in a manner that is consistent with the physical origin of the modes that they describe. However, the additional variation of the decay time of the fastest mode is required to match all simulation with all experiments consistently.

Upon comparing the time-integrated and the time-resolved photon echo experiments, the fact that the temperature dependence of 3PEPS data at 210 fs shows no evidence of the phase change at 150 K, whereas the HDPE results at the same waiting time do show this transition, is surprising. This is highly unexpected as both experiments are essentially sensitive to the same physical processes and therefore should yield comparable information. Furthermore, the EPS experiment is usually considered as a quick and simple means of obtaining the system dynamics. However, it completely fails to reveal the fundamental structural rearrangement that takes place during the glass transition that is clearly seen in the HDPE experiment at this particular waiting time.

This paradoxical situation can be understood by comparing the analytical expressions for both signals. Here we assume the same bimodal correlation function as used above in equation (3.17). After a Taylor expansion around t_w the relation between the slow part of the correlation function $M'_{slow}(t_w)$ that is sensitive to diffusive solvent dynamics and the echo peakshift function $t_{\max}(t_w)$ is expressed as:

$$aM'_{slow}(t_w) = \frac{\Delta\sqrt{\pi}\, t_{\max}(t_w)}{1+2\Delta^2 t^2_{\max}(t_w)}. \tag{6.16}$$

Assuming that the high-temperature limit applies and that $\Delta^2 t^2_{\max}(t_w) << 1$ this can be rewritten as

$$t_{\max}(t_w) = \frac{a\, M_{slow}(t_w)}{\Delta\sqrt{\pi}} \tag{6.17}$$

From here we derive the sensitivity of the EPS position to the balance between fast (homogeneous) and slow (inhomogeneous) modes, i.e. the parameter a:

$$\frac{\delta t_{\max}(t_w)}{\delta a} = \frac{M_{slow}(t_w)}{\Delta\sqrt{\pi}}\ . \tag{6.18}$$

For the HDPE experiment, the position of the maximum of the time-resolved echo signal with respect to the coherence time $t'_{\max}(\tau)$ can be expressed as:

$$t'_{\max}(\tau) = M'_{slow}(t_w)\tau - \frac{1-a}{a}\int_0^{t_{\max}} M'_{fast}(t_w)\,dt\ . \tag{6.19}$$

Similarly to equation (6.18), it follows that:

$$\frac{\delta t'_{\max}(\tau)}{\delta a} = \frac{\int_0^{\infty} M_{fast}(t_w)\,dt}{a^2}, \tag{6.20}$$

which serves as a handy indicator of the ratio between the fast and the slow modes.

Now we use equations (6.18) and (6.20) to estimate sensitivity of the 3PEPS and HDPE experiments to the balance between homogeneous and inhomogeneous contributions to the line broadening. Let us suppose that $M'_{slow}(t_w)$ is close to unity as it is the case for waiting times of $t_w = 210$ fs , and $\Delta = 0.05$ PHz (see Table 6.1). Then equation (6.18) yields:

$$\frac{\delta t_{\max}}{\delta a} = 10 \text{ fs} \tag{6.21}$$

The integral over the fast mode that enters equation (6.20), can be estimated as approximately equal to the correlation time, i.e. ≥ 100 fs at the temperatures around the glass transition, which results in

$$\frac{\delta t'_{\max}}{\delta a} = \frac{100}{a^2} \text{ fs}. \tag{6.22}$$

That is at least a decimal order of magnitude larger than equation (6.21). Therefore, changes in the ratio between the fast and the slow parts of the correlation function do have a much more profound impact on the time resolved HDPE signal as compared to the echo peakshift position. An additional consideration here is that the EPS depends on the amplitude of the environmental fluctuations Δ while the HDPE does not. The absorption spectrum narrows with the decrease of temperature, see Figure 6.1.a, adding to the 3PEPS the systematic temperature offset that masks the dynamics relevant information. In contrast, the HDPE experiment is free of such complications.

The fact that the 3PEPS is directly proportional to the ratio between the fast and slow parts of the correlation function can be used to strengthen the argument that the amplitude of the fast Gaussian mode has a strong temperature dependence. Below the glass temperature, the slow part of the correlation function is close to unity $M'(t_w) \approx 1$ at waiting times of $t_w = 210$ fs because the solvent motion is frozen, the damping of the 150 cm^{-1} vibrational mode is moderate, and not temperature-dependent any longer. Therefore, the 3PEPS function reflects mostly the balance between the relative amplitudes of the fast and slow part of the correlation function (never mind the ~25% changes in the absorption spectrum width).

6.4 Conclusions

In this chapter the effects of temperature on solvation dynamics were studied. The solvent, a glass-forming liquid, was cooled down from room temperature down to 3 K, a temperature range that includes the glass transition of this liquid at 150 K . The solvation dynamics were

studied by measuring the optical dephasing of a coherently excited ensemble of chromophores.

Temperature dependent optical dephasing in condensed matter has been studied several times before by others, but never over a temperature range this wide nor a range including a phase transition. For this reason, in these studies the results could be interpreted by either implicitly or explicitly assuming a SD that was temperature independent. Contrary to the experiments reported here, these studies used time integrated techniques like 2PE, 3PE and 3PEPS to measure the optical polarisation. In this chapter the echo signal was heterodyned using a local oscillator pulse in order to get a better insight in the ratio between fast and slow contributions to the optical dephasing. It is shown that it is not possible to do this with time integrated techniques only.

The 3PEPS results at a waiting time of 210 fs do not show signs of the glass transition because the solvent modes are too slow to have a noticeable effect on the peakshift at that time. This underlines the importance of time resolving the echo signal with a heterodyning field. In the HDPE results at the same waiting time, the glass transition is clearly discernible. This underlines the strengths of this technique; the heterodyned data allow for a much better separation of the contributions of the various modes. The HDPE technique can reveal dynamics that would have gone unnoticed in a time-integrated experiment.

The solvation dynamics of DTTCI in a PD/EtOH mixture can only be described with a temperature dependent SD. This is especially true above the glass transition temperature. The slowing down of molecular motion with decreasing temperature is clearly reflected in the characteristics of the corresponding MBO description. Even below the glass transition, when all solvent motion has vanished the SD is somewhat temperature dependent to make the behaviour of the inertial ultrafast contributions in the MBO-model reflect the experimental behaviour of the optical dephasing.

The description of the ultrafast mode was changed from the Gaussian character used by De Boeij *et al.* to a Gaussian correlation decay that is associated with a SD that linearly goes to zero at small wavelengths. The SD has to approach zero at the shortest wavelengths in this manner in order to have a description that yields reasonable polarisation decays.

Having modelled the correlation function by means of one fast mode, three intramolecular underdamped and four strongly damped solvent modes it is possible to simulate all the experiments, including absorption and emission profiles, at all temperatures with a reasonable degree of accuracy. This was done using a limited and closed set of BO-parameters that vary with temperature in a way that can be reasonably expected considering the physics involved.

From all this it can be concluded that especially time-resolved optical techniques are powerful tools in studying the ins and outs of solvation dynamics. Here it was shown that a

PD/EtOH mixture shows large aberrations from Arrhenius behaviour, and can therefore be considered a fragile liquid. The difficulty in studying solvation dynamics through optical dephasing lies in the precise characterisation of all the contributions to the correlation decay and the subsequent separation of intramolecular modes and solvent modes. The photon echo experiments are also inherently ensemble experiments and therefore not sensitive to the non-ergodic aspects of the glass transition and the solvation dynamics of the super-cooled liquid.